RESEARCH ARTICLE

Key Points:
- We thoroughly document an unusual sequence of Transient Luminous Events
- We present a universal method for reconstructing the current moment waveform
- Our method and results can be used to validate and improve TLE models

Correspondence to:
J. Mlynarczyk,
januszm@agh.edu.pl

An unusual sequence of sprites followed by a secondary TLE: An analysis of ELF radio measurements and optical observations

Janusz Mlynarczyk[1], József Bór[2], Andrzej Kulak[1,3], Martin Popek[4], and Jerzy Kubisz[3]

[1]Department of Electronics, AGH University of Science and Technology, Krakow, Poland, [2]Research Centre for Astronomy and Earth Sciences, GGI, Hungarian Academy of Sciences, Sopron, Hungary, [3]Astronomical Observatory, Jagiellonian University, Krakow, Poland, [4]AMSos, Eurosprite, Nýdek, Czech Republic

Abstract We present an extraordinary case of sprites in rapid succession—four sprite clusters in only 400 ms—followed by a secondary jet. Simultaneous ELF and optical observations, as well as lightning data, enabled us to thoroughly document this unique event. Locations of the transient luminous events (TLEs) were triangulated using video recordings from Nydek (Czech Republic) and Sopron (Hungary). We found that sprites were displaced up to 70 km from their parent lightning. The current moment waveform and charge moment changes associated with the event were reconstructed from the ELF electromagnetic signature recorded at the Hylaty station (Poland) by a new method. The results suggest that both a short-delayed and a long-delayed sprite were generated by a single positive cloud-to-ground discharge that had an intense continuing current. It had an unusual progression and lasted 200 ms. A large increase in the current moment during the development of a massive carrot sprite provides evidence in favor of sprite current. Our results also support the formation of an electric environment hypothesized to be necessary for the generation of the secondary TLEs.

1. Introduction

Transient luminous events (TLEs) are spectacular optical phenomena that occur above the clouds during thunderstorms [*Rodger*, 1999; *Inan*, 2002; *Mishin and Milikh*, 2008; *Inan et al.*, 2010; *Pasko*, 2010; *Pasko et al.*, 2012; *Surkov and Hayakawa*, 2012; *Siingh et al.*, 2012; *Ebert and Sentman*, 2008]. Since their discovery [*Franz et al.*, 1990], several types of TLEs have been documented and classified: sprites, blue jets, elves, gigantic jets, and others [*Sentman et al.*, 1995a, 1995b; *Fukunishi et al.*, 1996; *Su et al.*, 2003]. They have various shapes, sizes, and colors [*Lyons et al.*, 2003; *Williams*, 2001; *Neubert et al.*, 2008]. The mechanism of TLE generation is still not fully understood, but it is known to be closely linked with intense as well as impulsive charge separation and charge transfer processes in the troposphere [*Pasko et al.*, 2012]. Existing theoretical models are based on many optical observations from low-light cameras. These optical observations, however, are not always accompanied by reliable information on the current moment variation of the corresponding charge transfer processes, although this information is necessary to validate and improve the models.

In this paper, we analyze an unusual event that consisted of a sequence of sprites followed by a secondary TLE (a troll) in rapid succession. Secondary TLEs (also named crawlers, emblers, trolls, or secondary jets in the literature) [*Moudry*, 2003; *Marshall and Inan*, 2007] differ from "regular" TLEs—such as sprites and blue/gigantic jets—in that they develop in an electric environment which is preconditioned by a preceding sprite event. Forming such secondary TLEs is hypothesized to require the simultaneous presence of a lowered ionospheric potential (due to previous sprite currents) and a high concentration of charge in the thundercloud [*Lee et al.*, 2012], which occurs infrequently.

The TLEs considered in this paper were generated by intense lightning activity in a thunderstorm that moved across central Europe on 6 August 2013. We have analyzed extremely low frequency (ELF) radio recordings associated with the ground-based optical observations. Our ELF station was located only about 670 km away from the thunderstorm. Since the attenuation of ELF radio waves in the Earth-ionosphere waveguide is very low [*Kulak and Mlynarczyk*, 2013], such a distance can be considered short and enables the collection of high-quality waveforms (waveforms with high signal-to-noise ratios). Based on the recorded signal, we have reconstructed the complete current moment waveform of the TLE-associated discharges and calculated the charge moment change. To reconstruct the current moment waveform, a new method based on *Kulak and Młynarczyk* [2011] was used. This improved method makes it possible to avoid convolution, and it facilitates signal processing.
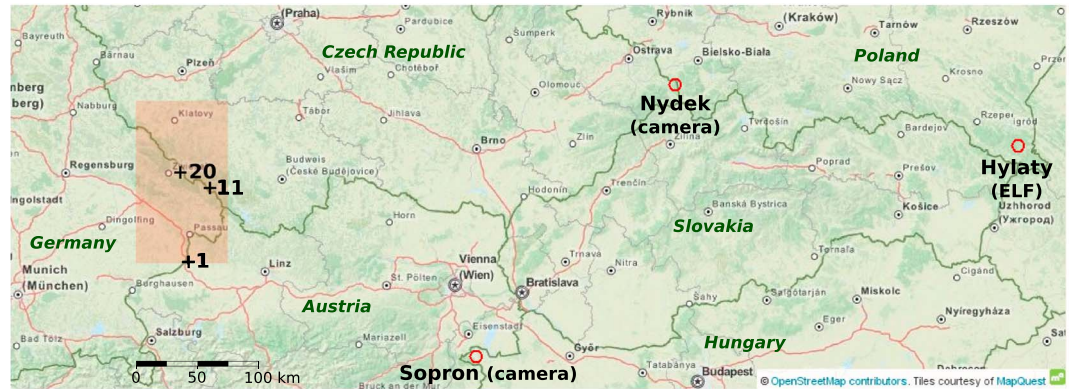
Figure 1. Location of the Hylaty ELF station and the cameras (Nydek and Sopron), as well as the location of the region where the sequence of TLEs occurred. The average distance from this region to the Hylaty ELF station was 670 km. The strongest +CG discharges, which played a major role in triggering sprites, are marked with plus signs and serial numbers (see Table 1 for details).

2. The Instrumentation and Radio Recordings

The ELF electromagnetic signature of the event was recorded by the Hylaty ELF station located in a sparsely populated area of the Bieszczady Mountains (49.204°N, 22.544°E) in Poland [*Kulak et al.*, 2014]. In this study, we use the data recorded by a receiver that has a frequency bandwidth of 0.03 to 52 Hz and a sampling frequency of 176 Hz. The receiver continuously measures two magnetic field components: NS (north-south) and EW (east-west).

The video images were recorded simultaneously at two sites: at Nydek, Czech Republic (49.668°N, 18.769°E) and at Sopron, Hungary (47.6837°N, 16.5830°E) [*Sátori et al.*, 2013]. The average distances from the recorded events were about 400 km and 320 km, respectively.

Figure 1 shows the locations of the observation sites and the region where the sequence of transient luminous events occurred. We also present the location of the positive cloud-to-ground (+CG) discharges that had the largest maximum current inferred from the VLF measurements (provided by LINET, Nowcast GmbH) [*Betz et al.*, 2009] and the largest amplitude in the ELF recordings (which translates into the highest current moments).

Figure 2 shows the ELF electromagnetic signature of the event recorded from two magnetic antennas, NS and EW, on 6 August 2013 at 22:34 UTC, after the propagation delay and receiver delay were subtracted. The average azimuth from the Hylaty ELF station to the discharge location was close to 270°. Therefore, the NS antenna was nearly perpendicular to the direction of propagation, and the +CG discharges are clearly visible
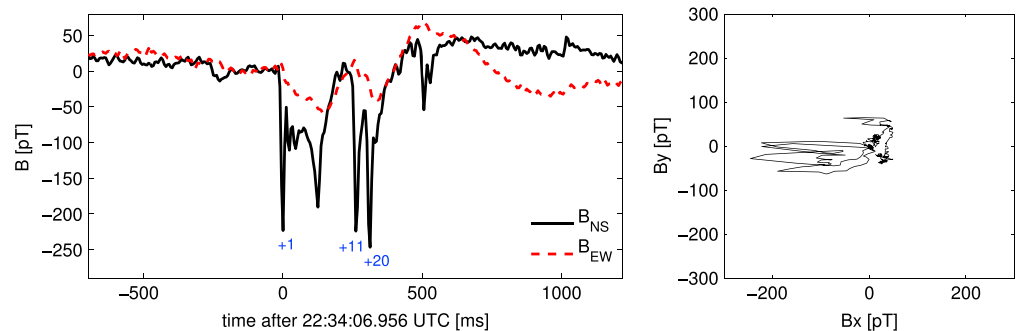

Figure 2. (left) Magnetic field components of the radio wave registered at the Hylaty ELF station by the north-south (red line) and east-west (blue line) antennas on 6 August 2013 at 22:34 UTC. The strongest +CG discharges are indicated by plus signs with serial number. (right) Lissajous pattern for the measured magnetic field components.
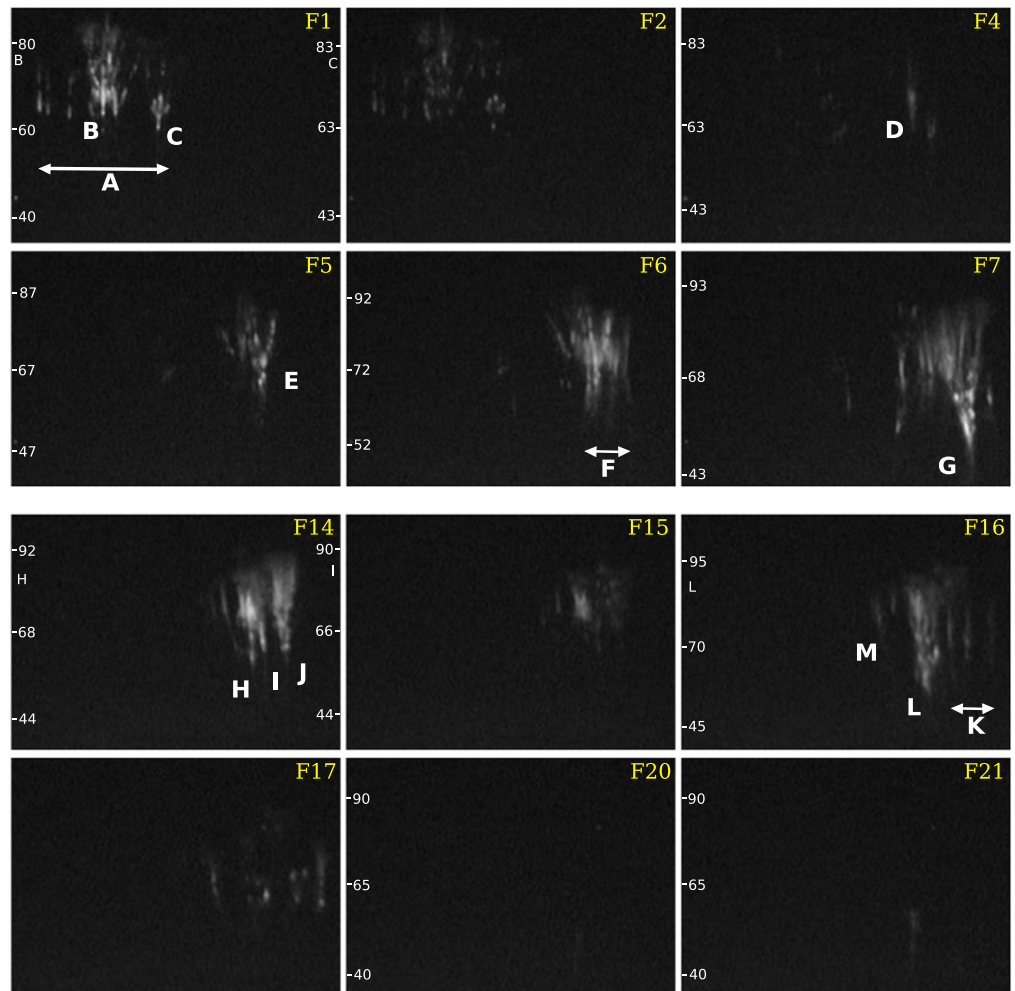
Figure 3. Selected video fields recorded at Sopron. Field number 1 (F1) was recorded at 22:34:06.969 UTC (±10 ms), and the following numbers correspond to 20 ms video fields. The capital letters identify various elements of the sprite clusters—their location can be followed on the map in Figure 3. (top) The first part of the recording. The same parts of the original video images were kept when cropping the pictures to preserve the relative position change of the sprites. (bottom) The second part of the recording. The same parts of the original images were kept for all the video fields in this panel, but they are different than in the top to keep the pictures small.

in the NS antenna but nearly invisible in the EW antenna. Negative amplitude in the plot in Figure 2 indicates the sources of positive polarity, e.g., positive cloud-to-ground discharges.

The video recordings at Nydek were made using Watec 910HX camera equipped with Computar 3.5–10.5 mm (F/1.0) lens. The recordings at Sopron were made with Watec 902H2 Ultimate with Computar 8 mm (F/0.8) lens. At both sites, video frames were recorded in 720 × 576 pixel optical resolution and at 50 video fields per second (deinterlaced) so that the effective time resolution at each site was 20 ms. The effective horizontal field of view is 45° in Sopron and 37° in Nydek. At Sopron station, a GPS video time inserter provided information on the start and end times of exposition period of each video field with millisecond accuracy. Both sites utilized the UFOCapture event detection and analyzer software package to capture transient optical phenomena and to process the records.

3. Analysis of Optical Records

The complex sequence of events analyzed in this paper can be divided into five parts, i.e., four sprite clusters followed by the troll. Because of the availability of simultaneous optical observations, the location and horizontal extension of each sprite cluster could be determined by triangulation. The location of the troll jet and some
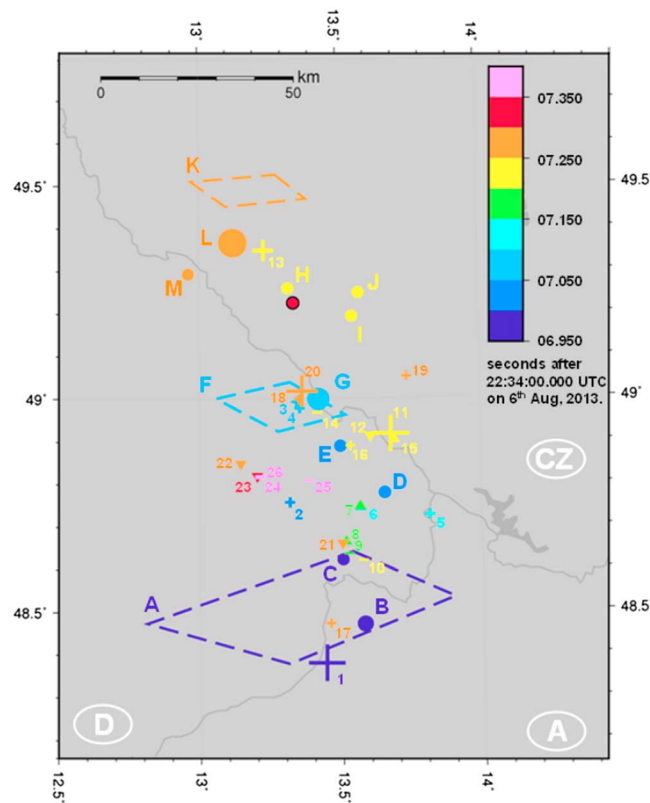
Figure 4. Triangulated locations of individual sprites (circles), triangulated areas of selected sprite groups (dashed lines), and locations of lightning flashes detected by LINET. The capital letters identify the emissions in Figure 3. The triangulated location of the troll jet is marked with a circle with a black outline. The numbers identify the lightning strokes in Table 1. The +CGs (cross), −CGs (minus sign), +ICs (triangle), and −ICs (inverted triangle) are plotted. Time is color coded. For the TLEs, the color corresponds to the time of the first appearance recognized in the video. (Larger sprites for which more entities could be triangulated individually are indicated with larger circles. The three largest crosses indicate the three strongest +CG discharges: 1, 11, and 20.)

individual sprite entities was triangulated, too, when the actual sprite entity could be unambiguously identified in both video records. To perform triangulation, the direction of selected characteristic points of the emissions was determined by finding the orientation of the image frame. The direction of the normal of the image plane was found by matching the stars in the field of view with the star chart at the time of observation using the UFOAnalyzer software. In Nydek, matching of the star chart was based on 41 stars, and the average and maximum deviations of recorded star directions from the corresponding directions in the star catalog were 0.012° and 0.039°, respectively. In Sopron, matching of the star chart was based on 22 stars, and the average and maximum direction deviations were 0.014° and 0.039°, respectively. Note that the number of stars available for direction finding depends both on the sensitivity of the recording systems (e.g., type of hardware and gain settings) and on local viewing conditions (e.g., light pollution and the level of atmospheric scattering). The accuracy of the triangulated locations is limited by the accuracy of the direction finding as well as by the finite optical resolution of the images. Additional uncertainty of the determined locations comes from the ambiguity in selecting the center and/or the edges of the emissions which do not have sharp

boundaries and can be somewhat out of focus too. An offset of 1 pixel corresponds to a 0.052° difference in Sopron and 0.041° in Nydek. Taking into account these factors as well as the distance of the events from the observation sites, we can say that true locations are supposed to be within a range of maximum 2 km of the triangulated locations.

The sequence of optical events can be followed in Figures 3 and 4. Figure 3 contains selected deinterlaced video fields of the event as recorded in Sopron, while triangulated locations are plotted in Figure 4. The sequence started with a very dim sprite halo at 22:34:06.949 UTC (±10 ms). Elements of the first cluster of sprites appeared together on the next video field (field 1; Figure 3). The cluster contained seven sprite entities of different types: columns, carrots, and trees. Note that we used the morphological classes discussed in details by *Bór* [2013] at the categorization of sprite entities according to their shape.

The appearance of the second set of sprites (video fields 4–7; Figure 3) cannot be unambiguously separated from the first cluster. The appearances of the entities closely followed one another, and the newer elements showed up laterally displaced from the earlier elements. Such a sequence of events is called "dancing" sprites in the literature [*Lyons*, 1994, 1996]. From 22:34:07.009 UTC (±10 ms, field 4; Figure 3), new sprite elements kept appearing on each new video field until field 7. Newer sprite entities appeared to the north of the previous entities. The shape of these sprites was again diverse. This cluster of dancing elements contained more than 10 sprite entities. Despite of the simultaneous observations from two sites, the

Table 1. Lightning Strokes Detected by LINET Above the Area Covered by the Map in Figure 4[a]

Serial	Time (UTC)	Longitude	Latitude	Type	I_{max} (kA)
1	**22:34:06.956**	**13.4445**	**48.3787**	**CG**	**81.8**
2	22:34:07.040	13.3198	48.7563	CG	5.8
3	22:34:07.071	13.3569	48.9771	CG	5.4
4	22:34:07.073	13.3458	48.9915	CG	6.8
5	22:34:07.131	13.8154	48.7257	CG	5.4
6	22:34:07.149	13.5703	48.7438	IC	4.6
7	22:34:07.171	13.5688	48.7462	IC	6.3
8	22:34:07.186	13.5179	48.6625	IC	6.9
9	22:34:07.199	13.5281	48.6351	CG	−5.6
10	22:34:07.210	13.5794	48.6198	CG	−5.3
11	**22:34:07.218**	**13.6803**	**48.9166**	**CG**	**37.7**
12	22:34:07.241	13.6073	48.9120	IC	−3.9
13	22:34:07.244	13.2315	49.3476	CG	11.6
14	22:34:07.248	13.4205	48.9672	CG	−8.5
15	22:34:07.249	13.6909	48.9027	IC	5.6
16	22:34:07.250	13.5360	48.8885	CG	4.7
17	22:34:07.251	13.4609	48.4716	CG	5.7
18	22:34:07.258	13.3540	48.9977	CG	5.7
19	22:34:07.261	13.7381	49.0504	CG	4.7
20	**22:34:07.266**	**13.3663**	**49.0167**	**CG**	**17.4**
21	22:34:07.267	13.5052	48.6589	IC	−4.8
22	22:34:07.279	13.1463	48.8475	IC	−5.2
23	22:34:07.338	13.2046	48.8182	IC	−8.2
24	22:34:07.360	13.2139	48.8145	CG	−7.2
25	22:34:07.368	13.3878	48.8072	CG	−7.6
26	22:34:07.385	13.2149	48.8182	CG	−6.3

[a]The three most powerful strokes (also displayed in Figure 1) are set in bold.

number of elements could not be determined unambiguously because of the densely packed cluster of many sprite entities (some of which were vertically tilted) and due to overlapping morphological features like glows, beads, and puffs. It must be noted that explicit beading could be observed in almost all sprite entities, even in columns and wishbones which has not been frequently observed at conventional frame rates. The lastly appearing large bright carrot was visible only for a single video field (≤20 ms). From this group, a previously appearing set of column sprites remained visible for the longest time (4 fields, 80 ms, from 22:34:07.049 to 22:34:07.129 UTC, ±10 ms).

The vanishing of those columns was followed by an 80 ms pause. Then, a closely packed group of two carrots and at least four other entities (columns and wishbones) appeared at 22:34:07.229 UTC (±10 ms, video field 14; Figure 3) to the north of the previous sprites. On the next video field, a great part of this cluster disappeared, while some emissions remained bright. On the following video field, 20 ms later, the last cluster of sprites appeared farther to the north. This cluster consisted of a large tree sprite and three to four columns (video field 16; Figure 3). The last optical remnants of these latter two clusters disappeared practically at the same time, i.e., at around 22:34:07.309 UTC (±10 ms).

Right after this, on the next video field (number 20; Figure 3) recorded at 22:34:07.329 UTC (±10 ms), the troll appeared practically below the third sprite cluster under the tendril region of one of the carrots. The troll was recorded on two video fields (40 ms) from Nydek and on three video fields (60 ms) from Sopron. The first two video fields (20 and 21; Figure 3) clearly show an upward development of the jet with its streamer channel remaining visible. On the second video field, a brighter spot could be observed along the upper part of the streamer channel. The top of the channel was also bright. By the third field, the streamer channel and the bright spots had disappeared, and only the very top of the channel was still faintly visible at the same height.

4. Lightning Activity and Optical Emissions

Table 1 contains information on lightning strokes above the area of the map in Figure 4 between 22:34:06.950 and 22:34:07.400 UTC on 6 August 2013. Figure 4 shows the LINET-reported location and time of these lightning strokes together with the triangulated locations of the emissions projected on the ground.
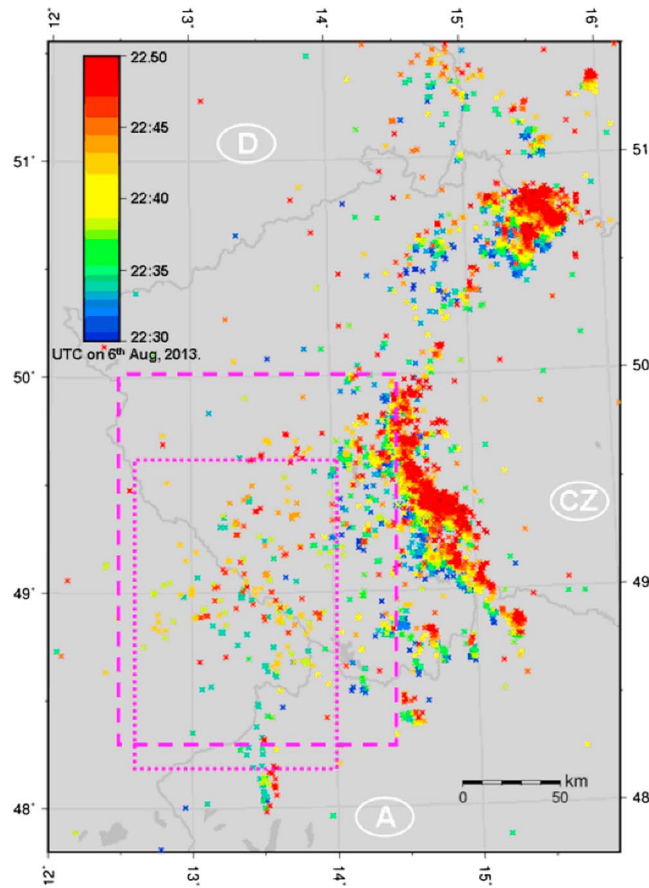
Figure 5. CG and IC lightning stroke locations detected by LINET. Time is color coded. The dashed magenta lines mark the area covered by Figure 4. The dotted magenta lines mark the latitude and longitude regions of 48.2–49.7 N, 12.6–14.0 E, in which lightning activity was more closely examined. See the corresponding text in the Discussion section.

Convective cells of the thunderstorm generally moved northeast near the occurrence time of the event considered in this study. The examined sequence of sprites, however, was generated by lightning activity in the trailing region of the thunderstorm, in which a northward drift was dominant at that time. This is well mirrored in the distribution and time evolution of lightning activity shown in Figure 5.

Considering the vicinity of the analyzed events, the region of lightning activity in general moved northward both in time and in space more or less synchronously with the appearing emissions, up to 22:34:07.266 UTC (Figure 4). Four +CG strokes with peak currents higher than 10 kA occurred in this period. These strokes were accompanied by several lightning strokes with smaller peak current (both CGs and intracloud (IC)) of dominantly positive polarity. All of the four negative strokes in this period occurred close (in time) to two larger peak current +CGs around 22:34:07.218 UTC. After the last bigger peak current +CG at 22:34:07.266 UTC, however, the detected lightning activity occurred only below 49.0° latitude and consisted of only negative polarity IC and CG strokes. No lightning stroke with a peak current higher than 10 kA was recorded in the region after this.

5. The Method for Reconstructing the Current Moment Waveform

The signal recorded by a receiver depends on the signal generated by the source, the transfer function of the propagation channel, and the transfer function of the receiving system. The first transfer function describes how the amplitude and phase of the radio wave change as it propagates from the source to the receiver's location. The second transfer function determines the amplitude and phase changes introduced by the receiving system.

This principle can be applied to any radio measurements. In this paper we apply it to the recordings of the magnetic field component of ELF radio waves generated by atmospheric discharges. Considering the signal in the frequency domain, we can write [*Kułak and Młynarczyk*, 2011]

$$\overline{B}(f) = \overline{s}(f)\,\overline{w}(f)\,\overline{g}(f) \quad [T/\text{Hz}], \tag{1}$$

where $\overline{B}(f)$ is the spectrum of the recorded magnetic field component of the radio wave, $\overline{s}(f)$ is the spectral density of the source current moment, $\overline{w}(f)$ in our case is the transfer function of the Earth-ionosphere waveguide, and $\overline{g}(f)$ is the transfer function of the ELF receiving system. All these parameters are complex, which we denote by macron above the letter.

The basic concept of our method is similar to that described by *Cummer and Inan* [2000] and *Kułak and Młynarczyk* [2011] in that it enables the reconstruction of an arbitrary current moment waveform from an ELF recording and obtain full information on the progression of the charge moment change during the event. The other well-known methods [*Jones*, 1970; *Burke and Jones*, 1996; *Sentman*, 1996; *Huang et al.*, 1999], which were also used in some recent papers on TLEs [*Soula et al.*, 2011; *Williams et al.*, 2007, 2012], require assuming an exponentially decaying current moment and, as it will become clear later, cannot be used for the case presented in this paper.

In order to reconstruct the current moment waveform, we have to take into account the radio wave propagation in the Earth-ionosphere waveguide and the influence of the receiver transfer function. *Cummer and Inan* [2000] calculated the impulse response of the propagation channel and reconstructed the current moment waveform by deconvolution. *Li et al.* [2008] used a modified version of this method to calculate the current moment waveform of sprites; they applied regularization parameters that enforce more smoothness on the later part of the current moment waveform. To avoid deconvolution-related issues, *Kułak and Młynarczyk* [2011] calculated the impulse response of the inverse channel and convolved it with the recorded waveform to obtain the current moment waveform.

In this paper, we avoid both convolution and deconvolution, making this method easy to implement. After obtaining all of the required parameters, as shown later in this section, we compute the spectrum of the current moment waveform, $\bar{s}(f)$, from equation (1), and we obtain the current moment waveform $s(t)$ by returning with $\bar{s}(f)$ to the time domain, using the inverse Fourier transform. All the calculations are implemented for the frequencies up to the Nyquist frequency (i.e., half of the sampling frequency of our ELF station). To obtain good resolution in the time domain for the current moment waveform, we work on two-sided spectra. (In order to convert one-sided spectrum to two-sided spectrum for a function calculated or measured only for positive frequencies, such as the receiver transfer function $\bar{g}(f)$, we use the complex conjugate).

Note that the method automatically removes the propagation delay of the Earth-ionosphere waveguide and the delay introduced by the receiver.

The transfer function of the Earth-ionosphere waveguide can be obtained from one of the well-known propagation formulas. In this paper, we use the equation presented by *Kułak and Młynarczyk* [2011], which is based on Banister's formula [*Casey*, 2002] and was derived analytically from the Maxwell equations for a vertical electric dipole placed in the Earth-ionosphere waveguide. It is well suited for calculating ELF radio wave propagation on relatively short distances, such as with the case shown in this paper. The transfer function $\overline{w}(f)$ is given by [*Kułak and Młynarczyk*, 2011]

$$\overline{w}(f) = -i \frac{\pi \mu_0 f}{2 h_m(f) v_{ph}(f)} H_1^{(2)} \left(2\pi r \frac{f}{v_{ph}(f)} \right) e^{-\alpha(f) r} \quad \left[\frac{T}{A \cdot m} \right], \tag{2}$$

where $h_m(f)$ is the magnetic altitude of the Earth-ionosphere waveguide, $v_{ph}(f)$ is the phase velocity of the electromagnetic wave in the waveguide, $H_1^{(2)}$ is the Hankel function of the second kind with order 1, r is the distance from the source, and $\alpha(f)$ is the attenuation rate of the waveguide.

In order to implement equation (2), we need to know the propagation parameters of the Earth-ionosphere waveguide. The phase velocity $v_{ph}(f)$ and the attenuation rate $\alpha(f)$ can be obtained from [*Mushtak and Williams*, 2002]

$$v_{ph}(f) = \frac{c}{\mathrm{Re}\,\overline{S}_o(f)}, \tag{3}$$

$$\alpha(f) = \frac{\omega}{c} \mathrm{Im}\,\overline{S}_o(f), \tag{4}$$

where $\overline{S}_o(f)$ is the complex propagation parameter. It can be estimated from the equation [*Mushtak and Williams*, 2002]

$$\overline{S}_o^{\,2}(f) = \frac{\overline{h}_m(f)}{\overline{h}_e(f)}, \tag{5}$$

where $\overline{h}_m(f)$ and $\overline{h}_e(f)$ are the complex magnetic and electric altitudes of the Earth-ionosphere waveguide. A detailed description of the complex propagation parameter and the complex altitudes can be found in *Kulak et al.* [2013].

The complex electric altitude can be calculated from the equations developed by *Greifinger et al.* [2007] and the magnetic altitude from the equations obtained by *Kułak and Młynarczyk* [2011, equation (9)] and *Kulak et al.* [2012, equation (11)] for the nighttime and daytime paths, respectively. These equations have shown a very good agreement with experimental data [*Kulak and Mlynarczyk*, 2013].

In order to calculate the spectral density of the current moment $\overline{s}(f)$ from the recorded magnetic field component $\overline{B}(f)$ using equation (1), we need to know one more parameter: the transfer function of the receiving system, $\overline{g}(f)$. The measurement system should be calibrated; therefore, its transfer function should be known in its entire frequency range.

A practical implementation of the presented method may require one more step. Many ELF systems, including the one we use, have two antennas: one directed north-south and the other east-west. In most cases, none of them is perpendicular to the direction of propagation. Therefore, we have to obtain the azimuthal magnetic field component, $\overline{B}(f)$, required by equation (1), from the magnetic field component recorded by the two antennas.

This can be done by a rotation of the coordinate system. For the given rotation angle α and a clockwise rotation, we can write

$$\begin{bmatrix} B \\ B_\| \end{bmatrix} = \begin{bmatrix} \cos(\alpha) & \sin(\alpha) \\ -\sin(\alpha) & \cos(\alpha) \end{bmatrix} \begin{bmatrix} B_x \\ B_y \end{bmatrix}. \tag{5}$$

Once the rotation is performed, we obtain the azimuthal magnetic field component with positive amplitude for +CG discharges. The rotation can be performed directly on the signal sampled in the time domain. Then we used the Fourier transform to calculate $\overline{B}(f)$ from B.

It should be stressed that the propagation models play an important role in estimating the amplitude of the current moment waveform. The method for reconstructing the current moment waveform shown in this paper is universal and enables us to use other models [e.g., *Jones*, 1970; *Sentman*, 1996; *Mushtak and Williams*, 2002]. However, we believe that the propagation formula used in this paper is well suited for calculating the magnetic field component of the radio waves at relatively short distances, such as in the case analyzed in this paper. The charge moment change (CMC) for cloud-to-ground return strokes obtained from our ELF records using this propagation formula have been recently compared with the CMCs derived from electrostatic analysis of electric field changes recorded by a network of VLF stations close to lightning locations, and a good correlation was obtained—the Pearson's cross-correlation coefficient for the negative return strokes was equal to 0.80 [*Nieckarz et al.*, 2015].

6. Results of Current Moment and Charge Moment Calculation

Figure 6 (top) shows the calculated current moment waveform. The parts of the waveform associated with video fields containing sprites are indicated with red lines. The troll video fields are indicated with a magenta line. The +CG discharges that played a major role in triggering sprites are marked with plus signs.

The first part of the current moment waveform has an unusual shape. It coincides with the dancing sprite event shown in Figure 3 (video fields 1 to 9), composed of two distinct clusters of sprites. After the return stroke of the first +CG discharge, which initiated the sequence ("+1" in Figure 6), the current did not decrease exponentially but remained at a quite high but constant level for about 80 ms. During this time, the first sprite cluster slowly vanished in the video recordings. Next, the current started to rise progressively, and the second cluster of sprites started to develop in the video recordings. The current moment reached the second maximum during video field 7. Then the current slowly decreased, reaching zero about 40 ms after the sprite cluster was no longer visible in the recordings. The first part of current moment waveform has some similarities to the current moment waveform presented by *Li et al.* [2008]. In their case, the amplitude of the first peak was about twice larger (~200 kA versus 90 kA), but then the amplitude decreased to about twice smaller value (roughly 20 kA versus 40 kA in our case), and then it increased to about 150 kA versus 75 kA in
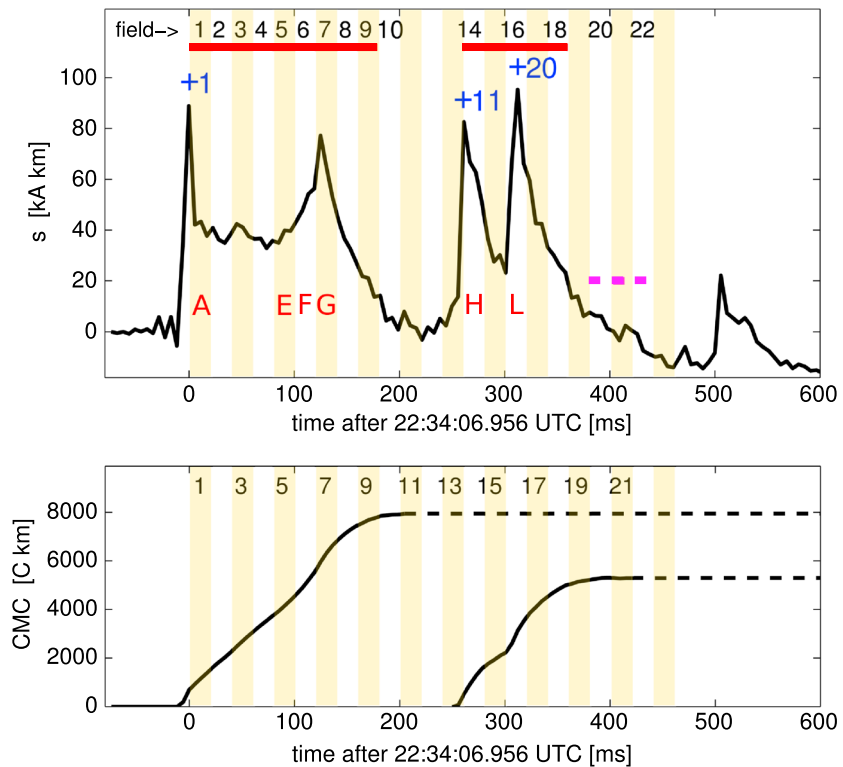
Figure 6. (top) The reconstructed current moment waveform. The parts of the waveform coinciding with sprite video field are indicated with red lines. The troll video fields are indicated with a magenta line. The strongest three +CG discharges are marked with plus signs. The video field number follows the same convention as in Figure 3. The capital letters indicate the selected sprite clusters shown in Figure 3. (bottom) Charge moment change derived by integration of the first and second parts of the current moment waveform. The first part (up to video field 10) coincides with the triggering +CG and the dancing sprite, and the second part (video fields 13–22) contains two strong +CG discharges, two sprite clusters, and the troll jet.

our case. The second peak in the current moment waveform in their case was ~145 ms after the first +CG, and in our case, it was after 125 ms.

After a short pause of about 40 ms, there was another strong +CG discharge and another cluster of sprites (the second part of the waveform, "+11" in field 14). The current dropped much faster than after the first +CG discharge, but before it settled, yet another strong +CG and sprite cluster appeared (video field 16 in Figures 3 and 6). This time, the current decreased more slowly, and before it settled, the troll jet appeared.

Signature of the next relatively strong +CG discharge of +18 kA peak current in this region is clearly visible in Figure 6, about 510 ms after the first +CG. Although it had a fairly slow current decay rate, our cameras did not record any TLE at that time.

Figure 6 (bottom) shows the vertical charge moment change (CMC) obtained by integration of the current moment waveform.

The charge moment change during the first part of the sequence (up to video field 10) was 7900 C km. This includes 700 C km associated with the return stroke of the first +CG discharge, 3200 C km associated with continuing current recorded during the first cluster of sprites (video fields 1 to 3), and 4100 C km during the second cluster of sprites (video fields 5 to 9).

The second part of the sequence started with a strong +CG discharge (second plus sign in Figure 6). Its return stroke had the charge moment change of 500 C km, and its continuing current during video fields 14 and 15 was 1700 C km. The charge moment change during video fields 16–19 (last sprite cluster) was 3000 C km. The CMC integrated during the rising edge of the current moment waveform in video field 16 was 900 C km. The main contribution to this CMC presumably comes from the return stroke of the 17.4 kA +CG. The charge moment change of the troll is difficult to estimate, because video frames 20 to 22 coincide also with negative IC

and CG discharges (numbers 23, 24, and 25 in Table 1 and Figure 4). The charge moment change associated with the whole second part of the sprite sequence (video fields 13–22) was 5300 C km.

The calculated charge moment change for the return strokes and the total charge moment change for each sprite event are within the range of values found by *Lu et al.* [2013]. They obtained the CMCs by integration of the current moment waveform, which was reconstructed by the deconvolution method of *Cummer and Inan* [2000]. *Williams et al.* [2007] obtained smaller CMC values; however, they did not reconstruct the current moment waveform but calculated the CMC using the method described by *Sentman* [1996], which requires the assumption that the charge transfer is short compared to round-the-world light time and has an exponentially decaying current.

Note that ELF measurements enable us to infer only the vertical component of the charge moment change. However, the vertical component is the key parameter in the initiation of sprites [*Asano et al.*, 2009]. Some recent theories suggest that a large charge moment change is a necessary but not sufficient condition for sprite initiation, and mesospheric irregularities might be a necessary condition for the initiation of sprite streamers [*Liu et al.*, 2012; *Kosar et al.*, 2012; *Qin et al.*, 2014], and that the sprite streamers can produce low-frequency electromagnetic radiation [*Qin et al.*, 2012; *Füllekrug et al.*, 2013].

7. Discussion

7.1. The First Part of the Sequence (the Dancing Sprite and the Delayed Sprites)

The initial sprite halo and the first sprite cluster were obviously triggered by the 81.8 kA +CG stroke at 22:34:06.956 UTC. The appearance of a sprite halo, observable with the applied set of hardware, suggests a parent lightning stroke with high peak current [*Williams et al.*, 2012]. Sprites of the first cluster appeared after their parent lightning stroke probably with a short delay (≤23 ms) [*Hu et al.*, 2007], which implies a large CMC during this discharge. Indeed, the estimated return stroke CMC of 700 C km exceeds the critical values for prompt sprite generation found in the U.S. by *Cummer and Lyons* [2005]. Sprites appeared north of the triggering lightning stroke. The three column sprites were probably the closest to the parent +CG stroke. The offset of the projected footprint of the brightest carrot sprite in the first cluster was 15–20 km, while the tree sprite on the far northern edge was displaced by about 35 km from the reported lightning stroke location (Figure 4).

No individual lightning strokes could be associated with each of the new sprite entities that appeared at the beginning of the sequence and made up the second cluster of sprites. A group of several column sprites (video field 6; Figure 3), on the other hand, appeared in the time window in which two small peak current +CGs were detected (strokes 3 and 4 in Table 1). The location of these lightning strokes coincides with the triangulated location of the sprite group.

Within the next 20 ms, a large carrot sprite appeared practically above the same area. The triggering mechanism of this bright sprite is not unambiguous. The two small peak current +CGs could hardly produce a CMC high enough for the initiation of short-delayed sprite events. A more plausible explanation is that the very strong continuing current following the return stroke of the first +CG continued to support the development of a mesospheric quasi-static electric field [*Li et al.*, 2008]. Fading of the elements of the first sprite cluster, subsequently appearing new sprite entities toward the north, and the smaller peak current discharges occurring again to the north support the idea that in-cloud current channels may have connected the discharge channel of the first +CG with other positive charge centers in the cloud.

In this case, elements of the second sprite cluster were rather delayed sprites, corresponding to the first +CG stroke. *Cummer and Füllekrug* [2001] reported on several cases when unusually long continuing currents of high amplitude indeed caused long-delayed sprites. Displacement of the big carrot sprite from the initial +CG stroke (~70 km) is in fair agreement with displacements found by *Füllekrug et al.* [2001] for long-delayed sprites as well as with those displacements estimated by *van der Velde et al.* [2010] in some cases of long-delayed sprites caused by horizontally extensive lightning discharges.

7.1.1. The Sprite Current

The sharp CM peak, coinciding with field 7 (Figure 6, top), is most probably due to the mesospheric current in the big carrot sprite [*Cummer et al.*, 1998; *Cummer*, 2003; *Hu et al.*, 2007]. The following facts support this interpretation. No lighting stoke anywhere within the LINET lighting detection network coincided with the

observed peak in the current moment waveform. The peak amplitude was very large; therefore, it is not very likely that it corresponded to a weak return stroke that was below the threshold of the VLF network. There were no time synchronization issues—the strokes detected by LINET were perfectly synchronized with their corresponding ELF signal. It can also be seen that the risetime for the suspected peak was much slower than for cloud-to-ground discharges. Examining the ELF signals from the two antennas (Figure 2), it is also clear that the peak in the magnetic field component suspected to be the sprite current can be barely seen in the signal registered by the EW antenna. We performed the antenna rotation using equation (5) and found that the angle between the direction of arrival of this signal and the location of the first return stroke (+1) was 6°. This coincides with the location of the big carrot sprite obtained from triangulation of the video recordings.

Early initiation and slow initial rising of this current peak are consistent with the observations of *Füllekrug et al.* [2001] ("slow variation") and *Li et al.* [2008] ("slow intensification" or SI), again in association with long-delayed sprites. *Li et al.* [2008] suggested that this charge moment (CM) feature can be a signature of extending discharge channels connecting and discharging further charge centers inside the thundercloud and leading to a net CMC high enough to generate long-delayed sprites. *Li et al.* [2008] doubted the relation of SI-type current variation to lightning *M* components. We note, however, that *M* components in +CG discharges may not be as impulsive as in −CG cases [*Campos et al.*, 2009], so in our opinion, an *M* component, too, may be considered as source of such a waveform. The small current enhancement at ~50 ms in Figure 6 can be another feature of this type. It is problematic to verify the validity of this idea without optical observations of the CG discharge channel. Nevertheless, we note that the potential role of lightning *M* components in sprite generation has been emphasized by modeling results of *Yashunin et al.* [2007] and *Asano et al.* [2009]. Additionally, it was observed that the previously appearing sprites in fields 5 and 6 in Figure 3 had the longest optical lifetime from this cluster and not the lastly appearing big carrot. This observation may indicate that the last big carrot sprite and the preceding set of sprites were produced by current processes of different time scales.

7.2. The Second Part of the Sequence (Two Sprites in Rapid Succession)

The appearance of the third sprite cluster was most probably triggered by the 37.7 kA +CG stroke ("+11" in Figure 6). The estimated high-return stroke CMC value of 500 C km suggests a short-delayed sprite event. The wider CM peak, on the other hand, can occur either because of a sprite current and/or a gradually decaying lightning current. The location of the appearing sprites was shifted by about 50 km to the north of the suspected parent stroke. Some of the sprites in this group may have remained bright due to a longer standing quasi-static mesospheric electric field supported by the 11.6 kA +CG stroke, which appeared only 26 ms after the previous big +CG. This smaller +CG stroke was also much closer to the location of the sprites than the original parent stroke.

The close temporal agreement between the appearance of the fourth sprite cluster and the 17.4 kA +CG stroke ("+20" in Figure 6) as well as the high initial CMC suggests that this event was also a short-delayed sprite. The wider CM peak can be interpreted similarly as in the previous case, but here the presence of a slowly decaying lightning current is more evident (Figure 6). The extended optical lifetime of some sprites and the experience that sprite currents are impulse like [*Cummer et al.*, 1998; *Füllekrug et al.*, 2001; *Li et al.*, 2008] support this finding.

We note that the amplitude of the horizontal displacement vector pointing to the last sprite cluster from its suspected parent stroke is of the same magnitude as the vector pointing from the first +CG to the last carrot in the second sprite cluster, as well as the displacement vector of the previous sprite event. These vectors are practically parallel to one another and point in the direction of the drifting of the lightning activity (Figure 5).

7.2.1. The Secondary TLE

A possible scenario of the secondary jet generation [*Marshall and Inan*, 2007; *Lee et al.*, 2012] is that the +CG discharge leaves an excess of negative charge in the cloud and the sprite current brings positive charge from the ionosphere to the base of the sprite cluster, forming the positive plate of a capacitor. The secondary jet is generated when the electric field exceeds the local breakdown level.

In our case, the troll jet occurred in the area below the third sprite cluster, practically halfway between the second and the fourth sprite clusters. If the CM waveform can be interpreted so that sprite current (section 7.1.1) occurred in all three sprite events, the ionospheric potential may have been lowered throughout a large area.

We note that no lightning stroke with a peak current larger than 10 kA was detected by LINET in the area corresponding to the analyzed events (the trailing region of the storm system, 48.2–49.7°N and 12.6–14.0°E;

marked with dotted magenta lines in Figure 5) for more than 4 min before the discussed events. However, nine CG strokes (seven positive and two negative) with peak currents larger than 10 kA were detected in the same area in 2 min just prior to that 4 min break (22:28–22:29 UTC).

This relatively long time interval without high peak current CG discharges can explain the accumulation of large amount of separated charge in the region, which could support the generation of the sprites as well as that of the secondary TLE. Long continuing currents after the three bigger +CGs must have created a considerable excess of negative charge in the thundercloud.

Since no lightning stroke was detected in the range of about 50 km of the location where the secondary jet appeared after the last strong +CG, this charge surplus must have remained there to facilitate the generation of the secondary jet. The time delay of the troll appearance after the big carrot sprite in the second cluster was less than 300 ms. This delay is much less than the few second mesospheric electric effect of sprites indicated by narrowband VLF detections [*Mika et al.*, 2005; *Haldoupis et al.*, 2010]. With these observations in mind, the joint analysis of triangulated sprite locations, the lightning data, and the CM variation inferred from the ELF measurements indirectly support the mechanism of secondary generation originally suggested by *Marshall and Inan* [2007].

7.3. Possible Excitation of Ionospheric Alfvén Resonator

The analyzed sequence of sprites was associated with a particular very low frequency waveform present in the EW antenna (see Figure 2), which was practically parallel to the direction of the analyzed event. This waveform is most probably due to the excitation of ionospheric Alfvén resonator (IAR) [*Sukhorukov and Stubbe*, 1997]. The IAR-associated waveform was called a ULF transient by *Sukhorukov and Stubbe* [1997] and was hypothesized to be a characteristic of sprite-associated discharges and manifest itself in the Earth-ionosphere waveguide. *Plyasov et al.* [2012] showed that the IAR spectra produced by a single lightning discharge can be observed on the ground and are present only in the radial component of the magnetic field. Our measurements provide evidence in favor of this theory.

8. Summary and Conclusions

In this paper, we have presented an impressive sequence of sprites that occurred in rapid succession and was followed by a secondary jet. We analyzed this event using our ELF and video recordings, as well as lightning data. The low-light video recorded simultaneously at two sites allowed us to determine the location of the TLEs. Lightning data helped us to characterize the lightning activity in the thunderstorm and to locate individual lightning stokes. Using the ELF data, we reconstructed the current moment waveform associated with the observed events. Combining these measurements enabled us to associate the current moment variations with their parent discharge processes and to obtain more information on charge transfer processes that generated the sprites and the secondary jet.

The analysis suggests that a single high peak current +CG (81.8 kA) generated two phenomena: a short-delayed cluster of sprites without obvious sprite current and a delayed sequence of sprites (dancing sprites) with a clearly detectable sprite current. Elements of the dancing sprite cluster were probably produced by the strong continuing current following the +CG return stroke. Slow intensification of the current before the detected sprite current suggests that an extension of the lightning channels may have occurred in the thundercloud during the continuing current phase of the discharge. This scenario can explain why the sprites appeared up to about 70 km from their parent lightning. The total CMC corresponding to this event was 7900 C km, where the return stroke of the +CG accounts for 700 C km, and 4100 C km can be associated with the suspected sprite current and the corresponding part of the subsequent continuing current.

Two more +CG lightning strokes of relatively higher peak current, 37.7 kA and 17.4 kA, followed the first intense +CG stroke after 262 ms and 310 ms, respectively. Coincident optical observations suggest that these lightning strokes produced short-delayed sprites. The total CMCs corresponding to these events were 2200 and 3000 C km, respectively. According to the corresponding CM waveform, considerable currents could flow in the body of these sprites. Provided that this scenario is valid, the slowly decaying current in the last +CG discharge and the subsequent absence of lightning activity in the region could create an environment that is suitable for the production of a secondary TLE by the mechanism suggested by *Marshall and Inan* [2007].

The presented analysis of this extraordinary sequence of TLEs demonstrates how involving more independent measurements and observations in an investigation can reveal multiple aspects of a phenomenon. In particular, we emphasize the importance of having reliable information on the charge transfer processes, and we have shown the usability of the described method to deduce charge moment variations from ELF records. It is worth noting that the Hylaty ELF station has a lower cutoff frequency of only 0.03 Hz, which is lower than most other ELF stations in the world. This enables us to record very slow electromagnetic field changes generated by long-lasting continuing currents, such as the current associated with the dancing sprite shown in this paper. If the lower cutoff frequency were significantly higher, a large part of the continuing current would be invisible due to bandwidth limitations.

References

Asano, T., T. Suzuki, Y. Hiraki, E. Mareev, M. G. Cho, and M. Hayakawa (2009), Computer simulations on sprite initiation for realistic lightning models with higher-frequency surges, *J. Geophys. Res.*, *114*, A02310, doi:10.1029/2008JA013651.

Betz, H.-D., K. Schmidt, and W. P. Oettinger (2009), LINET: An International VLF/LF Lightning Detection Network in Europe, in *Lightning: Principles, Instruments, and Applications*, Chap. 5, edited by H.-D. Betz, U. Schumann, and P. Laroche, pp. 115–140, Springer, Netherlands, doi:10.1007/978-1-4020-9079-0.

Bór, J. (2013), Optically perceptible characteristics of sprites observed in central Europe in 2007–2009, *J. Atmos. Sol.-Terr. Phys.*, *92*, 151–177, doi:10.1016/j.jastp.2012.10.008.

Burke, C. P., and D. L. Jones (1996), On the polarity and continuing currents in unusually large lightning flashes deduced from ELF events, *J. Atmos. Terr. Phys.*, *58*, 531–540, doi:10.1016/0021-9169(95)00054-2.

Campos, L. Z. S., M. M. F. Saba, O. Pinto Jr., and M. G. Ballarotti (2009), Waveshapes of continuing currents and properties of M components in natural positive cloud-to-ground lightning, *Atmos. Res.*, *91*(2–4), 416–424, doi:10.1016/j.atmosres.2008.02.020.

Casey, J. P. (2002), Extremely low frequency (ELF) propagation formulas for dipole sources radiating in a spherical Earth-ionosphere waveguide, *NUWC-NPT Tech. Rep. 11*, Nav. Undersea Warfare Cent. Div., Newport, R. I.

Cummer, S. A. (2003), Current moment in sprite-producing lightning, *J. Atmos. Sol.-Terr. Phys.*, *65*, 499–508.

Cummer, S. A., and M. Füllekrug (2001), Unusually intense continuing current in lightning produces delayed mesospheric breakdown, *Geophys. Res. Lett.*, *28*(3), 495–498, doi:10.1029/2000GL012214.

Cummer, S. A., and U. S. Inan (2000), Modeling ELF radio atmospheric propagation and extracting lightning currents from ELF observations, *Radio Sci.*, *35*(2), 385–394, doi:10.1029/1999RS002184.

Cummer, S. A., and W. A. Lyons (2005), Implications of lightning charge moment changes for sprite initiation, *J. Geophys. Res.*, *110*, A04304, doi:10.1029/2004JA010812.

Cummer, S. A., U. S. Inan, T. F. Bell, and C. P. Barrington-Leigh (1998), ELF radiation produced by electrical currents in sprites, *Geophys. Res. Lett.*, *25*(8), 1281–1284, doi:10.1029/98GL50937.

Ebert, U., and D. Sentman (2008), Editorial review: Streamers, sprites, leaders and lightning from micro to macroscales, *J. Phys. D Appl. Phys.*, *41*, 230301.

Franz, R. C., R. J. Nemzak, and J. R. Winkler (1990), Television image of a large upward electrical discharge above a thunderstorm system, *Science*, *249*, 48–51.

Fukunishi, H. Y., Y. Takahashi, M. Kubota, K. Sakanoi, U. S. Inan, and W. A. Lyons (1996), Elves: Lightning-induced transient luminous events in the lower ionosphere, *Geophys. Res. Lett.*, *23*, 2157, doi:10.1029/96GL01979.

Füllekrug, M., D. R. Moudry, G. Dawes, and D. D. Sentman (2001), Mesospheric sprite current triangulation, *J. Geophys. Res.*, *106*(D17), 20,189–20,194, doi:10.1029/2001JD900075.

Füllekrug, M., A. Mezentsev, S. Soula, O. Van Der Velde, and T. Farges (2013), Sprites in low-frequency radio noise, *Geophys. Res. Lett.*, *40*, 2395–2399, doi:10.1002/grl.50408.

Greifinger, P. S., V. C. Mushtak, and E. R. Williams (2007), On modeling the lower characteristic ELF altitude from aeronomical data, *Radio Sci.*, *42*, RS2S12, doi:10.1029/2006RS003500.

Haldoupis, C., N. Amvrosiadi, B. R. T. Cotts, O. A. van der Velde, O. Chanrion, and T. Neubert (2010), More evidence for a one-to-one correlation between sprites and early VLF perturbations, *J. Geophys. Res.*, *115*, A07304, doi:10.1029/2009JA015165.

Hu, W., S. A. Cummer, and W. A. Lyons (2007), Testing sprite initiation theory using lightning measurements and modeled electromagnetic fields, *J. Geophys. Res.*, *112*, D13115, doi:10.1029/2006JD007939.

Huang, E., E. Williams, R. Boldi, S. Heckman, W. Lyons, M. Taylor, T. Nelson, and C. Wong (1999), Criteria for sprites and elves based on Schumann resonance observations, *J. Geophys. Res.*, *104*, 16,943–16,964, doi:10.1029/1999JD900139.

Inan, U. S. (2002), Lightning effects at high altitudes: Sprites, elves, and terrestrial gamma ray flashes, *C. R. Phys.*, *3*(10), 1411–1421.

Inan, U. S., S. A. Cummer, and R. A. Marshall (2010), A survey of ELF and VLF research on lightning-ionosphere interactions and causative discharges, *J. Geophys. Res.*, *115*, A00E36, doi:10.1029/2009JA014775.

Jones, D. L. (1970), Numerical computations of terrestrial ELF electromagnetic wavefields in the frequency domain, *Radio Sci.*, *5*(5), 803–809, doi:10.1029/RS005i005p00803.

Kosar, B. C., N. Liu, and H. K. Rassoul (2012), Luminosity and propagation characteristics of sprite streamers initiated from small ionospheric disturbances at subbreakdown conditions, *J. Geophys. Res.*, *117*, A08328, doi:10.1029/2012JA017632.

Kułak, A., and J. Młynarczyk (2011), A new technique for reconstruction of the current moment waveform related to a gigantic jet from the magnetic field component recorded by an ELF station, *Radio Sci.*, *46*, RS2016, doi:10.1029/2010RS004475.

Kulak, A., and J. Mlynarczyk (2013), ELF propagation parameters for the ground-ionosphere waveguide with finite ground conductivity, *IEEE Trans. Antennas Propag.*, *61*(4), 2269–2275.

Kulak, A., J. Mlynarczyk, M. Ostrowski, J. Kubisz, and A. Michalec (2012), Analysis of ELF electromagnetic field pulses recorded by the Hylaty station coinciding with terrestrial gamma ray flashes, *J. Geophys. Res.*, *117*, D18203, doi:10.1029/2012JD018205.

Kulak, A., J. Młynarczyk, and J. Kozakiewicz (2013), An analytical model of ELF radiowave propagation in ground-ionosphere waveguides with a multilayered ground, *IEEE Trans. Antennas Propag.*, *61*(9), 4803–4809.

Kulak, A., J. Kubisz, S. Klucjasz, A. Michalec, J. Mlynarczyk, Z. Nieckarz, M. Ostrowski, and S. Zieba (2014), Extremely low frequency electromagnetic field measurements at the Hylaty station and methodology of signal analysis, *Radio Sci.*, 49, 361–370, doi:10.1002/2014RS005400.

Lee, L.-J., S.-M. Huang, J.-K. Chou, C.-L. Kuo, A. B. Chen, H.-T. Su, R.-R. Hsu, H. U. Frey, Y. Takahashi, and L.-C. Lee (2012), Characteristics and generation of secondary jets and secondary gigantic jets, *J. Geophys. Res.*, 117, A06317, doi:10.1029/2011JA017443.

Li, J., S. A. Cummer, W. A. Lyons, and T. E. Nelson (2008), Coordinated analysis of delayed sprites with high-speed images and remote electromagnetic fields, *J. Geophys. Res.*, 113, D20206, doi:10.1029/2008JD010008.

Liu, N., B. Kosar, S. Sadighi, J. R. Dwyer, and H. K. Rassoul (2012), Formation of streamer discharges from an isolated ionization column at subbreakdown conditions, *Phys. Rev. Lett.*, 109, 025002, doi:10.1103/PhysRevLett.109.025002.

Lu, G., et al. (2013), Coordinated observations of sprites and in-cloud lightning flash structure, *J. Geophys. Res. Atmos.*, 118, 6607–6632, doi:10.1002/jgrd.50459.

Lyons, W. A. (1994), Characteristics of luminous structures in the stratosphere above thunderstorms as imaged by low-light video, *Geophys. Res. Lett.*, 21, 875–878, doi:10.1029/94GL00560.

Lyons, W. A. (1996), Sprite observations above the U.S. High Plains in relation to their parent thunderstorm systems, *J. Geophys. Res.*, 101, 29,641–29, 652, doi:10.1029/96JD01866.

Lyons, W. A., T. E. Nelson, R. A. Armstrong, V. P. Pasko, and M. A. Stanley (2003), Upward electrical discharges from thunderstorm tops, *Bull. Am. Meteorol. Soc.*, 84(4), 445–454, doi:10.1175/BAMS-84-4-445.

Marshall, R. A., and U. S. Inan (2007), Possible direct cloud-to-ionosphere current evidenced by sprite-initiated secondary TLEs, *Geophys. Res. Lett.*, 34, L05806, doi:10.1029/2006GL028511.

Mika, A., C. Haldoupis, R. A. Marshall, T. Neubert, and U. S. Inan (2005), Subionospheric VLF signatures and their association with sprites observed during EuroSprite-2003, *J. Atmos. Sol.-Terr. Phys.*, 67, 1580–1597, doi:10.1016/j.jastp.2005.08.011.

Mishin, E. V., and G. M. Milikh (2008), Blue jets:Upward lightning, *Space Sci. Rev.*, 137(1–4), 473–488.

Moudry, D. (2003), The dynamics and morphology of sprites, ProQuest Dissertations And Theses; thesis (PhD)-University of Alaska Fairbanks; Publication Number: AAI3092292; ISBN:9780496399994; Source: Dissertation Abstracts International, Volume: 64–05, Section: B, page: 2233; 155 pp. [Available at http://adsabs.harvard.edu/abs/2003PhDT........88M.]

Mushtak, V. C., and E. R. Williams (2002), ELF propagation parameters for uniform models of the Earth-ionosphere waveguide, *J. Atmos. Sol. Terr. Phys.*, 64, 1989–2001.

Neubert, T., et al. (2008), Recent results from studies of electric discharges in the mesosphere, *Surv. Geophys.*, 29, 71–137.

Nieckarz, Z., P. Baranski, J. Mlynarczyk, A. Kulak, and J. Wiszniowski (2015), Comparison of the charge moment change calculated from electrostatic analysis and from ELF radio observations, *J. Geophys. Res. Atmos.*, 120, 63–72, doi:10.1002/2014JD022289.

Pasko, V. P. (2010), Recent advances in theory of transient luminous events, *J. Geophys. Res.*, 115, A00E35, doi:10.1029/2009JA014860.

Pasko, V. P., Y. Yair, and C.-L. Kuo (2012), Lightning related transient luminous events at high altitude in the Earth's atmosphere: Phenomenology, mechanisms, and effects, *Space Sci. Rev.*, 168, 475–516, doi:10.1007/s11214-011-9813-9.

Plyasov, A. A., V. V. Surkov, V. A. Pilipenko, E. N. Fedorov, and V. N. Ignatov (2012), Spatial structure of the electromagnetic field inside the ionospheric Alfvén resonator excited by atmospheric lightning activity, *J. Geophys. Res.*, 117, A09306, doi:10.1029/2012JA017577.

Qin, J., S. Celestin, and V. P. Pasko (2012), Low-frequency electromagnetic radiation from sprite streamers, *Geophys. Res. Lett.*, 39, L22803, doi:10.1029/2012GL053991.

Qin, J., V. P. Pasko, M. G. McHarg, and H. C. Stenbaek-Nielsen (2014), Plasma irregularities in the *D* region ionosphere in association with sprite streamer initiation, *Nat. Commun.*, 5, 3740, doi:10.1038/ncomms4740.

Rodger, C. (1999), Red sprites, upward lightning, and VLF perturbations, *Rev Geophys*, 37(3), 317–336, doi:10.1029/1999RG900006.

Sátori, G., M. Rycroft, P. Bencze, F. Märcz, J. Bór, V. Barta, T. Nagy, and K. Kovács (2013), An overview of thunderstorm-related research on the atmospheric electric field, Schumann resonances, sprites, and the ionosphere at Sopron, Hungary, *Surv. Geophys.*, 34(3), 255–292, doi:10.1007/s10712-013-9222-6.

Sentman, D. D. (1996), Schumann resonance spectra in a two-scale-height Earth-ionosphere cavity, *J. Geophys. Res.*, 101, 9479–9488, doi:10.1029/95JD03301.

Sentman, D. D., E. M. Wescott, D. L. Osborne, D. L. Hampton, and M. J. Heavner (1995a), Preliminary results from the Sprites94 aircraft campaign: 1. Red sprites, *Geophys. Res. Lett.*, 22, 1205–1208, doi:10.1029/95GL00583.

Sentman, D. D., E. M. Wescott, D. L. Osborne, D. L. Hampton, and M. J. Heavner (1995b), Preliminary results from the sprites 94 aircraft campaign: 2. Blue jets, *Geophys. Res. Lett.*, 22, 1209–1213, doi:10.1029/95GL00582.

Siingh, D., R. P. Singh, A. K. Singh, S. Kumar, M. N. Kulkarni, and A. K. Singh (2012), Discharges in the stratosphere and mesosphere, *Space Sci. Rev.*, 169(1–4), 73–121, doi:10.1007/s11214-012-9906-0.

Soula, S., O. van der Velde, J. Montanya, P. Huet, C. Barthe, and J. Bór (2011), Gigantic jets produced by an isolated tropical thunderstorm near Réunion Island, *J. Geophys. Res.*, 116, D19103, doi:10.1029/2010JD015581.

Su, H. T., R. R. Hsu, A. B. Chen, Y. C. Wang, W. S. Hsiao, W. C. Lai, L. C. Lee, M. Sato, and H. Fukunishi (2003), Gigantic jets between a thundercloud and the ionosphere, *Nature*, 423, 974–976.

Sukhorukov, A. I., and P. Stubbe (1997), Excitation of the ionospheric resonator by strong lightning discharges, *Geophys. Res. Lett.*, 24, 829–832, doi:10.1029/97GL00807.

Surkov, V. V., and M. Hayakawa (2012), Underlying mechanisms of transient luminous events: A review, *Ann. Geophys.*, 30, 1185–1212.

van der Velde, O. A., J. Montanyà, S. Soula, N. Pineda, and J. Bech (2010), Spatial and temporal evolution of horizontally extensive lightning discharges associated with sprite-producing positive cloud-to-ground flashes in northeastern Spain, *J. Geophys. Res.*, 115, A00E56, doi:10.1029/2009JA014773.

Williams, E., et al. (2012), Resolution of the sprite polarity paradox: The role of halos, *Radio Sci.*, 47, RS2002, doi:10.1029/2011RS004794.

Williams, E. R. (2001), Sprites, elves, and glow discharge tubes, *Phys. Today*, 54, 41–47.

Williams, E. R., V. C. Mushtak, R. Boldi, R. L. Dowden, and Z.-I. Kawasaki (2007), Sprite lightning heard round the world by Schumann resonance methods, *Radio Sci.*, 42, RS2S20, doi:10.1029/2006RS003498.

Yashunin, S. A., E. A. Mareev, and V. A. Rakov (2007), Are lightning *M* components capable of initiating sprites and sprite halos?, *J. Geophys. Res.*, 112, D10109, doi:10.1029/2006JD007631.